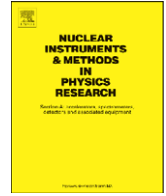




Contents lists available at ScienceDirect

# Nuclear Instruments and Methods in Physics Research A

journal homepage: [www.elsevier.com/locate/nima](http://www.elsevier.com/locate/nima)

## Neutron signals for dual-readout calorimetry

N. Akchurin<sup>a</sup>, M. Alwarawrah<sup>a</sup>, A. Cardini<sup>b</sup>, G. Ciapetti<sup>c</sup>, R. Ferrari<sup>d</sup>, S. Franchino<sup>d</sup>, M. Fraternali<sup>d</sup>, G. Gaudio<sup>d</sup>, J. Hauptman<sup>e</sup>, F. Lacava<sup>c</sup>, L. La Rotonda<sup>f</sup>, M. Livan<sup>d</sup>, E. Meoni<sup>f</sup>, D. Pinci<sup>c</sup>, A. Policicchio<sup>f</sup>, S. Popescu<sup>a</sup>, G. Susinno<sup>f</sup>, Y. Roh<sup>a</sup>, W. Vandelli<sup>g</sup>, T. Venturelli<sup>f</sup>, C. Voena<sup>c</sup>, I. Volobouev<sup>a</sup>, R. Wigmans<sup>a,\*</sup>

<sup>a</sup> Texas Tech University, Lubbock, TX, USA<sup>b</sup> Dipartimento di Fisica, Università di Cagliari and INFN Sezione di Cagliari, Italy<sup>c</sup> Dipartimento di Fisica, Università di Roma "La Sapienza" and INFN Sezione di Roma, Italy<sup>d</sup> Dipartimento di Fisica Nucleare e Teorica, Università di Pavia and INFN Sezione di Pavia, Italy<sup>e</sup> Iowa State University, Ames, IA, USA<sup>f</sup> Dipartimento di Fisica, Università della Calabria and INFN Cosenza, Italy<sup>g</sup> CERN, Genève, Switzerland

### ARTICLE INFO

#### Article history:

Received 24 June 2008

Received in revised form

10 September 2008

Accepted 14 September 2008

Available online 17 October 2008

#### Keywords:

Calorimetry

Cherenkov light

Optical fibers

Neutron signals

### ABSTRACT

The contributions of neutrons to hadronic signals from the DREAM calorimeter are measured by analyzing the time structure of these signals. This contribution is characterized by an exponential tail in the pulse shape, with a time constant of  $\sim 20$  ns. The relative contribution of neutrons to the signals is measured event by event. It is shown that this information can be used to improve the hadronic calorimeter performance.

© 2008 Elsevier B.V. All rights reserved.

## 1. Introduction

The precision with which the energy of hadrons and jets can be measured with instruments based on total absorption of this energy (calorimeters) is ultimately limited by fluctuations in nuclear binding energy losses that occur in the numerous nuclear reactions that take place in the absorption process. The energy needed to release nucleons and nuclear aggregates (e.g.,  $\alpha$  particles) from nuclei in the absorber structure does not contribute to the measurable signals, and is thus usually referred to as *invisible energy*. It may, on average, amount to more than 20% of the total energy carried by the showering object, with large event-to-event fluctuations about this average [1].

It has been demonstrated that efficient detection of the neutrons released in the absorption process may strongly reduce the effects of these fluctuations, and thus lead to an important improvement of the hadronic energy resolution. This is the basic reason why compensating calorimeters based on efficient neutron detection [2,3] have a considerably better energy resolution than

uranium/liquid-argon calorimeters with a similar  $e/h$  value [4,5]. Measurements by the ZEUS Collaboration have shown that efficient neutron detection may reduce the intrinsic limit of the hadronic energy resolution in (Pb/plastic-scintillator) calorimeters to  $< 0.15E^{-1/2}$  [6].

In a previous paper [7], we have demonstrated that it is possible to measure the contributions of neutrons to the hadron signals from our DREAM fiber calorimeter, using the time structure of these signals. The neutrons, which mainly originate from the evaporation stage of nuclear breakup in the hadronic shower development process, contribute through elastic scattering off protons in the plastic scintillating fibers which provide the  $dE/dx$  information in this calorimeter. Their contribution is characterized by an exponential tail in the pulse shape, with a time constant of  $\sim 20$  ns.

In the present study, we have investigated to what extent event-by-event information on the contribution of neutrons to the signals can be used to improve the hadronic calorimeter performance. In Section 2, we describe the calorimeter, the experimental setup in which it was tested, and the techniques used to extract the desired information from the signals. Experimental results are presented and discussed in Section 3. Summarizing conclusions are given in Section 4.

\*Corresponding author. Tel.: +1806 742 3779; fax: +1806 742 1182.

E-mail addresses: [wigmans@ttu.edu](mailto:wigmans@ttu.edu), [Richard.Wigmans@ttu.edu](mailto:Richard.Wigmans@ttu.edu) (R. Wigmans).

## 2. Equipment and measurements

### 2.1. The detector

The detector used for our studies is the DREAM calorimeter, which has been described in considerable detail elsewhere [8–10]. The characteristic aspect of this calorimeter is its capability to measure simultaneously both the total deposited energy, and the energy deposited by the relativistic charged shower particles [11], hence the name (DREAM stands for Dual REAdout Method). The basic element of this detector (see Fig. 1) is an extruded copper rod, 2 m long and  $4 \times 4 \text{ mm}^2$  in cross-section. This rod is hollow, and the central cylinder has a diameter of 2.5 mm. Seven optical fibers were inserted in this hole. Three of these were plastic scintillating fibers, the other four fibers were undoped and intended for detecting Cherenkov light.

The DREAM detector consisted of 5580 such rods, 5130 of these were equipped with fibers. The empty rods were used as fillers, on the periphery of the detector. The instrumented volume thus had a length of 2.0 m, an effective radius of 16.2 cm, and a mass of 1030 kg. The calorimeter's radiation length ( $X_0$ ) was 20.1 mm, its Molière radius ( $\rho_M$ ) 20.4 mm and its nuclear interaction length ( $\lambda_{\text{int}}$ ) 200 mm.

The fibers were grouped to form 19 readout towers. Each tower consisted of 270 rods and had an approximately hexagonal shape (80 mm apex to apex). The effective radius of each tower was 37.1 mm ( $1.82\rho_M$ ). A central tower (#1) was surrounded by two hexagonal rings, the Inner Ring (six towers, numbered 2–7) and the Outer Ring (12 towers, numbered 8–19). The towers were not segmented in the longitudinal direction.

The fibers leaving the rear of this structure were separated into bunches: one bunch of scintillating fibers and one bunch of Cherenkov fibers for each tower, 38 bunches in total. In this way, the readout structure was established (see Fig. 1). Each bunch was coupled through a 2 mm air gap to a photomultiplier tube (PMT).<sup>1</sup> Much more information about this calorimeter is provided in Refs. [8–10].

### 2.2. The beam line

The measurements described in this paper were performed in the H4 beam line of the Super Proton Synchrotron at CERN. The DREAM detector was mounted on a platform that could move vertically and sideways with respect to the beam. For the measurements described here, we only used one detector position, namely where the beam entered the detector parallel to its axis (the “0” orientation) in its geometrical center, i.e., in the center of Tower #1.

An important goal of these measurements was to study the signals, not only from single particles, but also from jets. To this end, a 10 cm ( $0.1\lambda_{\text{int}}$ ) thick polyethylene target (IT) was installed about 50 cm upstream of the calorimeter. The signals from a plastic scintillator plane (PMTi, see Fig. 2) were used to select beam particle interactions in this target. The size of these signals was used as an indication of the multiplicity of these interactions. By selecting such interactions, we could study the calorimeter signals for events in which several particles entered the detector simultaneously. Of course, the composition of the events selected this way was typically quite different from that of fragmenting quarks or gluons. However, in the absence of a *jet test beam*, these multi-particle events exhibited a calorimetrically very important characteristic: in these events, a number of different particles

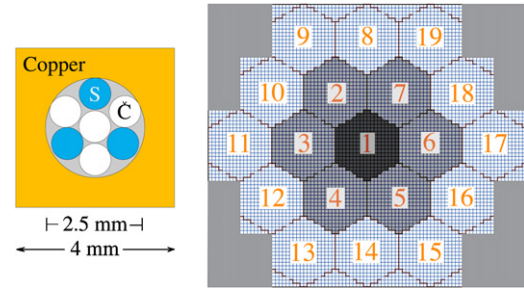


**Fig. 1.** The basic building block of the DREAM calorimeter is a  $4 \times 4 \text{ mm}^2$  extruded hollow copper rod of 2 m length, with a 2.5 mm diameter central hole. Seven optical fibers (four undoped and three scintillating fibers) with a diameter of 0.8 mm each are inserted in this hole, as shown in the left diagram. The right diagram shows a cross-section of the calorimeter, which consists of 19 hexagonal towers.

with different energies entered the detector simultaneously, the properties of these individual components were not known, but their total energy was (approximately) known.<sup>2</sup> In the following, we will refer to these multi-particle events as “jets”.

Two small scintillation counters provided the signals that were used to trigger the data acquisition system. These Trigger Counters (TC) were 2.5 mm thick, and the area of overlap was  $6 \times 6 \text{ cm}^2$ . A coincidence between the logic signals from these counters provided the trigger. The trajectories of individual beam particles could be reconstructed with the information provided by two small drift chambers (DC1, DC2) which were installed upstream of the TCs. This system made it possible to determine the location of the impact point of the beam particles at the calorimeter surface with a precision of typically  $\sim 0.2 \text{ mm}$ . About 10 m downstream of the IT, placed behind about 20 interaction lengths of material, a  $50 \times 50 \text{ cm}^2$  scintillator paddle served as a muon counter.

### 2.3. Data acquisition

Measurement of the time structure of the calorimeter signals was the primary goal of the tests described here. In order to limit distortion of this structure as much as possible, we used special 15 mm thick low-loss cables to transport the calorimeter signals to the counting room. Such cables were also used for the signals from the TCs, and these were routed such as to minimize delays in the DAQ system.<sup>3</sup> The signals that were not subject to time structure measurements (e.g., from PMTi and the muon counter) were transported through RG-58 cables with (for timing purposes) appropriate lengths to the counting room, where they were fed into charge ADCs.

The data acquisition system used VME electronics. A single VME crate hosted all the needed readout and control boards. The charge measurements were performed with a CAEN V792AC QADC module,<sup>4</sup> that offered 12-bit digitization at a sensitivity of 100 fC/count and a conversion time below 10  $\mu\text{s}$ . The signals from the muon counters were integrated and digitized with a sensitivity of 100 fC/count, on a 12-bit LeCroy 1182 module.<sup>5</sup> The timing information of the tracking chambers was recorded with 1 ns resolution in a 16-bit 16-channel LeCroy 1176 TDC.<sup>6</sup>

<sup>2</sup> Absorption inside the target and the production of secondaries at large angles, which may have physically missed the calorimeter, were responsible for a small uncertainty in the energy deposited in the calorimeter.

<sup>3</sup> We measured the signal speed to be 0.78c in these cables.

<sup>4</sup> [http://www.caen.it/nuclear/Printable/data\\_sheet.php?mod=V792&fam=vme&fun=qdc](http://www.caen.it/nuclear/Printable/data_sheet.php?mod=V792&fam=vme&fun=qdc)

<sup>5</sup> <http://lecroy.com/lrs/dsheets/1182.htm>

<sup>6</sup> <http://www.lecroy.com/lrs/dsheets/1176.htm>

<sup>1</sup> Hamamatsu R-580, a 10-stage, 1.5" PMT with a nominal gain of  $3.7 \times 10^5$  at 1250 V.

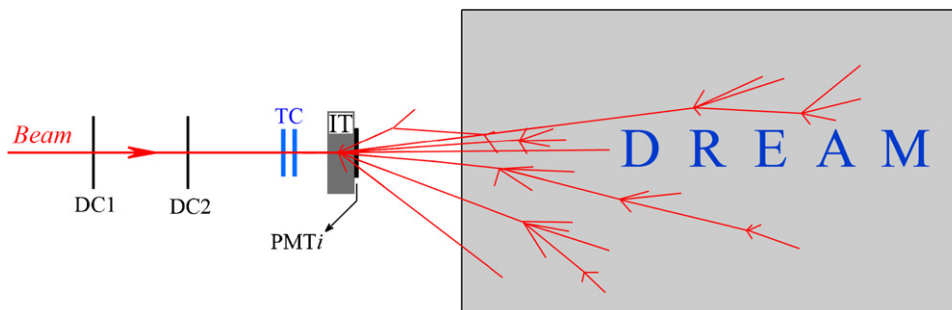


**Fig. 2.** Schematic (not to scale) of the experimental setup in which the contribution of neutrons to the signals from the DREAM fiber calorimeter were measured. Not shown is a  $50 \times 50 \text{ cm}^2$  scintillation counter placed 8 m downstream of the calorimeter, which served as a muon counter.

The time structure of the calorimeter signals was recorded by means of a Tektronix TDS 7254B digital oscilloscope,<sup>7</sup> which provided a sampling capability of 5 GSamples/s, at an analog bandwidth of 2.5 GHz, over four input channels. During this data taking period, four channels were sampled, at a rate of 1.25 GS/s (0.8 ns sampling) over a time interval of 224 ns. The oscilloscope gain (scale) was tuned such as to optimize the exploitation of the 8-bit dynamic range, i.e., by choosing the sensitivity such that the overflow rate was  $\leq 1\%$ .

The trigger logic was implemented through NIM modules and the signals were sent to a VME I/O register, which was also catching the spill and the global busy information. The VME crate was linked to a data acquisition computer through an SBS 620 optical VME-PCI interface.<sup>8</sup> This computer was equipped with a Pentium-4 2 GHz CPU, 1 GB of RAM, and running a CERN SLC 4.3 operating system.<sup>9</sup>

The data acquisition was built around a single-event polling mechanism and performed by a readout program that was streaming physics and on-spill pedestal events into two independent first-in-first-out buffers, built on top of 32 MB shared memories. Our readout scheme optimized the CPU utilization and increased the data taking efficiency thanks to the bunch structure of the SPS cycle, where beam particles were provided to our experiment during a spill of 4.8 s, with a repetition period of 16.8 s.

Owing to the large volume of data produced by the oscilloscope and the poor on-line performance of this instrument, we decided to use it on a multi-event basis. Through the GPIB interface, the digital scope was prepared to acquire events before the extraction and delivery of protons on target. On spill, all events were sequentially recorded in the internal memory of the scope. At the end of the spill, the oscilloscope memory was dumped onto a temporary file, in a network-mounted shared disk. At this point, the file was read out and the data copied in properly-formatted areas in the shared-memory buffers, where the information from all the VME modules had already been stored, in real time, by the readout program. In sequence, the recorder programs were then dumping the events to disk and a monitoring program was running in spy mode, on top of the physics shared memory, producing online histograms.

With this scheme, we were able to reach, in spill, a data acquisition rate of  $\sim 2 \text{ kHz}$ , limited by the size of the internal scope buffer. No zero suppression was implemented, so that the event size was constant:  $\sim 1.5 \text{ MB}$ , largely dominated by the oscilloscope data.

#### 2.4. Calibration of the detector signals

Before proceeding to the time structure measurements, the gains of all 38 PMTs reading out the scintillation and Cherenkov signals from the 19 calorimeter towers were individually equalized. Using the high voltage, the gain in all PMTs was set to generate 1 pC/GeV. This was done with 50 GeV electrons, which were steered into each of the 19 towers.

The showers generated by these particles were not completely contained in a single calorimeter tower. The (average) containment was found from EGS4 Monte Carlo simulations. When the electrons entered a tower in its geometrical center, on average 92.5% of the scintillation light and 93.6% of the Cherenkov light was generated in that tower [8]. The remaining fraction of the light was shared by the surrounding towers. The signals observed in the exposed tower thus corresponded to an energy deposit of 46.3 GeV in the case of the scintillating fibers and of 46.8 GeV for the Cherenkov fibers.

After the gains of the individual PMTs were equalized in this way, we also had to calibrate the energy scale of the oscilloscope channels. This was done with 50 GeV electrons as well. The electrons were sent into the central tower, and the signals from the scintillator and Cherenkov channels (equivalent to 46.3 and 46.8 GeV, respectively) were determined by integrating over the entire time structure. This procedure was repeated for each of the four input channels of the oscilloscope.

#### 2.5. Experimental data and procedures

A major goal of this experiment was to obtain information about the *total* neutron production in the events. This in contrast with the measurements described in Ref. [7], where the time structure of signals from individual towers was studied, for towers located at different distances from the shower axis. In order to achieve the stated goal, signals from different towers were added by means of a Linear Adder, and the summed pulses were sampled by the oscilloscope. We took great care in making sure that the individual signals arrived simultaneously at the Adder input, differences in PMT transit time were compensated by means of cable length. Four signals were formed in this way:

- (1) The scintillator signal from Tower #1 ( $S_1$ ).
- (2) The scintillator signal from the *inner ring* ( $\sum S_i$ , with  $i = 2-7$ ).
- (3) The scintillator signal from the *outer ring* ( $\sum S_j$ , with  $j = 8-19$ ).
- (4) The Cherenkov signal:  $\sum Q_k$ , with  $k = 1-16$ .

Since the Linear Adder had only 16 inputs, signals from three towers from the Outer Ring were not included in the Cherenkov

<sup>7</sup> [http://www.tek.com/site/ps/0,55-13766-SPECS\\_EN,00.html](http://www.tek.com/site/ps/0,55-13766-SPECS_EN,00.html)

<sup>8</sup> <http://www.gefanucembedded.com/products/457>

<sup>9</sup> <http://linux.web.cern.ch/linux/scientific4/>

sum. This had some consequences for the energy calibration. Since this calibration was carried out with electrons in Tower #1, the contribution of the three “missing” towers to the calibration signals was negligible. However, to determine the energy equivalent of hadron and jet signals to which these three towers did contribute, we multiplied the measured Cherenkov signals by a factor  $\frac{19}{16}$ . Since absolute energy measurements played no significant role in the analyses described in this paper, the consequences of this approximation are very limited.

The four signals listed above were sent into the four input channels of the oscilloscope and sampled for each event.

Data were collected for three beam energies: Positive pions at 100, 200 and 300 GeV. For each energy, 500 000 events were collected. Since the interaction target represented  $0.1\lambda_{\text{int}}$ , these included about 50 000 “jets” and 450 000 “single pions”. The distinction was made on the basis of the signal in PMTi. Fig. 3 shows the signal distribution in this scintillator plane, on a logarithmic scale, for 200 GeV pions. The most probable signal value corresponded to 80 ADC counts above pedestal. We will refer to this signal as “1 mip”, since it was the most likely signal produced by a pion that traversed the IT target without causing a nuclear interaction. The threshold for “jets” was set at 1000 ADC counts, i.e.,  $\sim 12$  mip. The probability that a non-interacting pion would cause such a signal was found (from the Landau distribution in this scintillator plane with the target removed) to be  $< 1\%$ . This means that  $> 90\%$  of the selected events indeed represented pions interacting in the IT target.

One may wonder to what extent the cut in signals from the IT counter biased our event samples, and in particular the em fraction (i.e., the  $\pi^0$  content) of the events. We have investigated this issue in several ways. A simple, straightforward experimental answer was obtained by comparing the ratios of the total signals in the Cherenkov and scintillating fibers for event samples with different cuts on the IT signal. As we have shown in Ref. [9], this ratio ( $Q/S$ ) is strongly correlated with the em shower fraction, and thus with the  $\pi^0$  content of the events (see also Eq. (2)). It turned out that the em shower fraction was only very slightly affected by a cut on the IT signal. If the threshold was increased from 300 ADC counts (a multiplicity of about 4) to 3000 ADC counts (a multiplicity of 40), the average em shower fraction of the selected events decreased by about 5%. For the threshold used by us (1000 ADC counts, i.e., a multiplicity of 12), the average em shower fraction was lower than that for a cut at 300 ADC counts by less than 1%.

The fact that the em shower fraction was barely affected by the cut on the IT signal can be understood by realizing that the

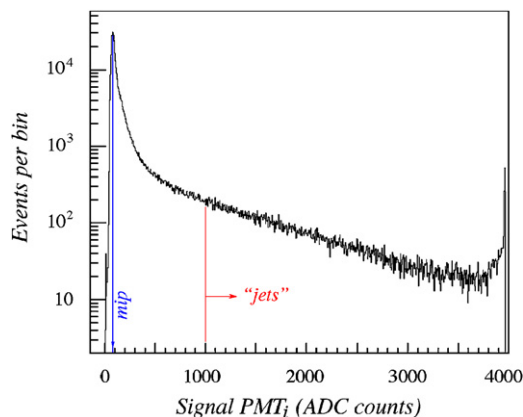


**Fig. 3.** Signal distribution in the PMTi scintillation counter for 200 GeV pions. Events producing a signal in excess of 1000 ADC counts were classified as a multiparticle (“jet”) event in this analysis.

probability that  $\pi^0$ 's produced in upstream interactions contributed to the signals from the IT counter was by no means negligible. If one of the  $\gamma$ 's from a decaying  $\pi^0$  converts upstream of the counter, the result is a signal contribution with an amplitude of 2 mip. If both  $\gamma$ 's convert, the resulting contribution to the IT signal is equivalent to 4 mip. Even larger signal contributions are possible as a result of radiation emitted by the electrons/positrons produced in the conversion process. Simulations with a GEANT4 Monte Carlo confirmed that the mentioned bias in our “jet” event sample was indeed insignificant.

Off-line, the beam chamber information could be used to select events that entered the target in a small (typically  $10 \times 10 \text{ mm}^2$ ) region located around its geometric center. The pion beam contained a few percent of muons, which were eliminated either with help of the downstream muon counter, or on the basis of the total (mip) signal they generated in the calorimeter.<sup>10</sup> Typically, more than half of the events survived these cuts.

### 3. Experimental results

#### 3.1. Neutrons and the time structure of the signals

The measurements performed for the present study were in a number of ways different from the ones that were used earlier to establish the presence of a neutron component in the signals. These differences can be summarized as follows:

- The measurements were not limited to individual towers, but integrated over the entire detector.
- Simultaneous information on the time structure of the Cherenkov and scintillation signals from the same events was obtained.
- The measurements were performed with a better time resolution (0.8 vs. 2.5 ns), and the signals were followed over a longer time interval.
- Experimental data were collected not only for single pions, but also for multi-particle events (“jets”).

The benefits of the improved time resolution are illustrated in Fig. 4, which shows the average time structure of signals recorded for 200 GeV “jets”, on a logarithmic scale. The Cherenkov signals (integrated over 16 calorimeter towers) were very fast, the pulse height dropped by an order of magnitude in about 10 ns. The scintillator signals, integrated here over the Inner + Outer Rings (Towers 2–19), exhibited the characteristic two-component structure also observed in our previous study [7]. The two components correspond to decay times of about 9 and 20 ns. The latter component is the result of slow (few-MeV) neutrons which lost their kinetic energy through elastic collisions with hydrogen nuclei in the plastic fibers. As expected, there was no sign of such a tail in the time structure of the signals from the Cherenkov fibers, since the recoil protons produced in this process were non-relativistic.

The origin of the tail in the scintillation signals became very clear when we compared the magnitude of this tail in the three scintillation signals from which the time structure was recorded simultaneously. For the 200 GeV “jet” events considered here, the signal portion integrated from  $t = 20\text{--}40$  ns represented, on average, 10% of the total signal from the central tower, 17% for the total signal from the Inner Ring and 20% for the total signal from the Outer Ring (see Fig. 1). In other words, moving away from

<sup>10</sup> Multiple scattering caused some muons to miss the downstream muon counter, especially at the lowest energies.

the shower axis, the neutrons represented an increasing fraction of the measured signal. This should be expected on the basis of the fact that the neutrons (unlike the pions produced in the shower) were not traveling in any preferred direction and because of their relatively large mean free path between subsequent elastic collisions. Similar observations for signals from individual towers in our previous studies led us to conclude that the tail in the time structure exhibits indeed the characteristics expected from a neutron component [7].

### 3.2. Neutrons in individual events

The signal from the Inner + Outer Rings integrated from  $t = 20\text{--}40\text{ ns}$  also formed the basis for the event-by-event

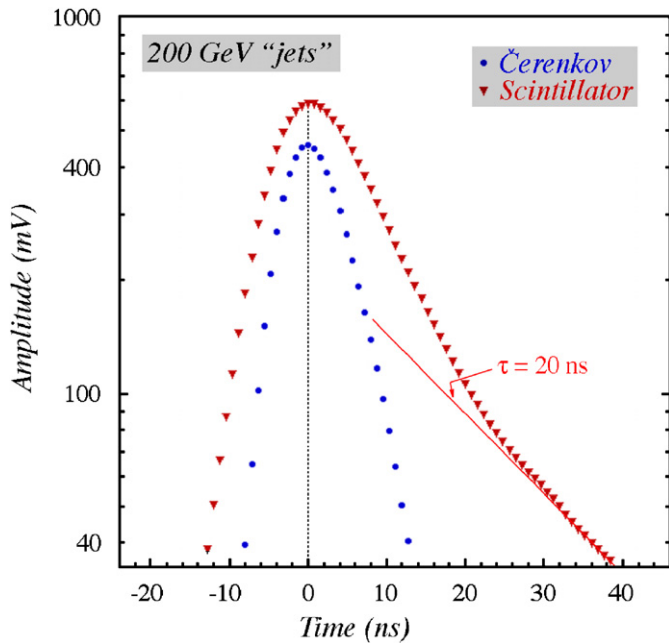


**Fig. 4.** Average time structure of the Cherenkov and scintillation signals recorded for 200 GeV “jets” developing in the DREAM calorimeter. The scintillation signals exhibit a tail with a time constant of about 20 ns, which is absent in the Cherenkov signals.

determination of the neutron contribution to the total scintillator signal, and for the analysis described below.

Fig. 5a shows the event-by-event distribution of this signal for the 200 GeV “jet” event sample, while Fig. 5b depicts the event-by-event distribution of the fraction of the total scintillator signal represented by the signals from Fig. 5a. We will refer to this fraction in the following as  $f_n$ , which is thus defined as

$$f_n = \frac{\int_{t=20\text{ ns}}^{40\text{ ns}} \sum_{i=2}^{19} S_i}{\int_{t=0}^{\infty} \sum_{i=1}^{19} S_i}. \quad (1)$$

Fig. 5b shows that  $f_n$ , defined in this way, varied between 0.04 and 0.10. There are of course many other ways in which the neutron fraction could possibly be defined. We have explored various other choices, and found that the conclusions of the analysis described in the following were not affected by this particular definition of  $f_n$ .

### 3.3. The neutron fraction and other event characteristics

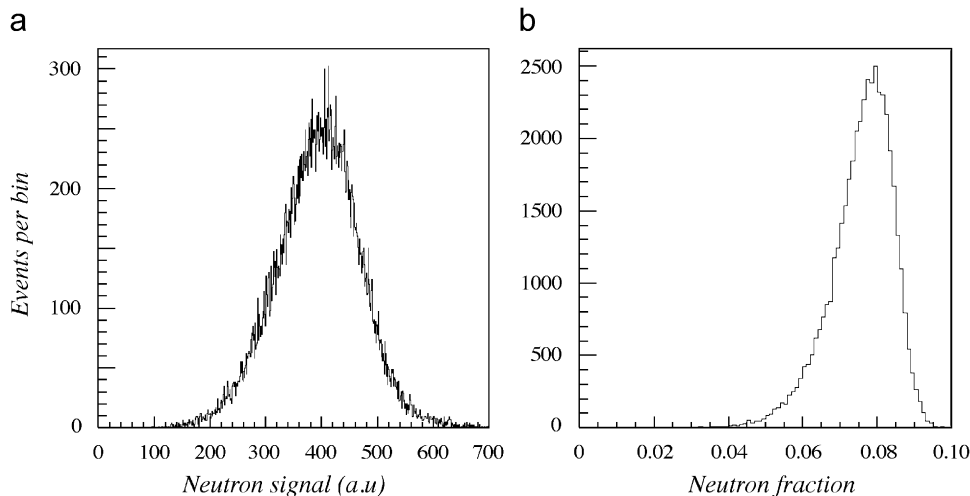
A major purpose of the present study was to investigate if and to what extent event-by-event measurements of the neutron content of the signals could provide information about the invisible energy and thus might be used to improve the hadronic performance of the calorimeter.

Fig. 6 shows a scatter plot in which the relationship between the neutron fraction, as defined in Eq. (1), and the total Cherenkov signal is displayed, for the 200 GeV “jet” event sample. Each dot represents one event from this sample. The figure shows a very clear (anti-)correlation between the total Cherenkov signal and the fractional contribution of neutrons to the total scintillator signal: the larger the neutron fraction, the smaller the total Cherenkov signal. Since neutrons, as we saw before (Fig. 4), did not contribute to the Cherenkov signal, this result should not come as a surprise.

Perhaps more interesting is Fig. 7. In this scatter plot, the relationship between  $f_n$  and the total Cherenkov/scintillator signal ratio (the so-called  $Q/S$  ratio) is displayed. This  $Q/S$  ratio is directly related to the electromagnetic shower fraction,  $f_{em}$ , as

$$\frac{Q}{S} = \frac{f_{em} + 0.21(1 - f_{em})}{f_{em} + 0.77(1 - f_{em})} = \frac{0.21 + 0.79f_{em}}{0.77 + 0.23f_{em}} \quad (2)$$

where 0.21 and 0.77 represent the  $h/e$  values of the Cu/quartz and Cu/scintillator calorimeter structures [9]. Therefore, as  $f_{em}$  varies



**Fig. 5.** The contribution of neutrons to the total hadronic scintillator signals from 200 GeV “jets”. Shown are the event-by-event distributions of the signals integrated from  $t = 20\text{--}40\text{ ns}$  in the Inner + Outer Rings (a) and of the fraction of the total scintillator signal represented by this signal component (b).

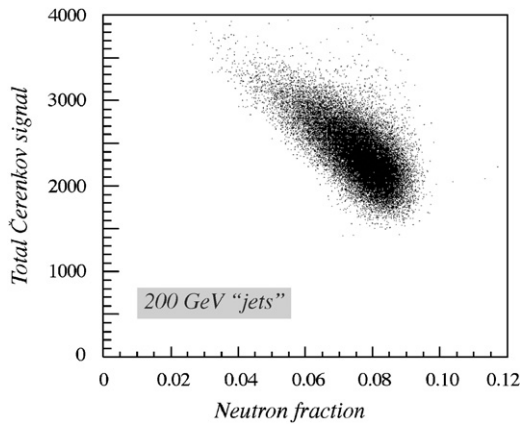


**Fig. 6.** Scatter plot for 200 GeV “jets”. For each event, the combination of the total Cherenkov signal and the fractional contribution of neutrons to the total scintillator signal is represented by a dot. The neutron fraction was determined according to Eq. (1).

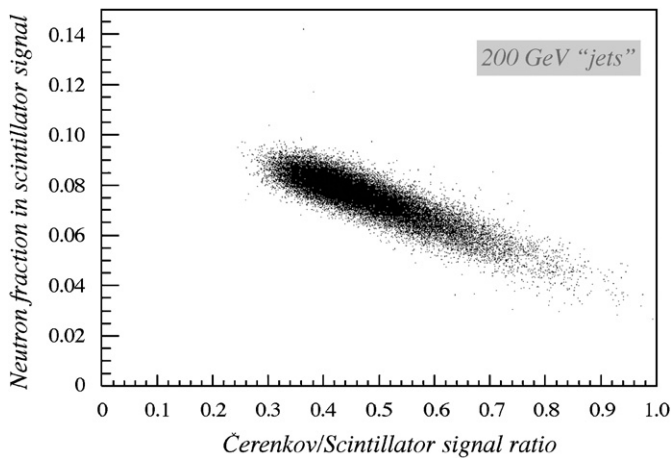


**Fig. 7.** Scatter plot for 200 GeV “jets”. For each event, the combination of the total Cherenkov/scintillator signal ratio and the fractional contribution of neutrons to the total scintillator signal is represented by a dot. The neutron fraction was determined according to Eq. (1).

between 0 and 1,  $Q/S$  varies between 0.27 and 1. The scatter plot shows that as the fraction of the energy of the showering object that ended up in the form of em ( $\pi^0$ ) shower components increased, the relative contribution of neutrons to the total scintillator signal decreased. Since (almost) no neutrons were produced in the em shower component, also this result should not come as a surprise.

However, these results have very interesting consequences. A crucial feature of the dual-readout technique is the possibility to measure the em shower fraction event by event by comparing the signals from two different media with very different  $e/h$  values (Eq. (2)). By measuring this fraction event by event, the effects of its (large and non-Gaussian) fluctuations on the hadronic calorimeter resolution can be eliminated [9]. However, because of the strong (anti-)correlation between the fractional contribution of neutrons to the total scintillator signal ( $f_n$ ) on the one hand, and the  $Q/S$  signal ratio, and thus the em shower fraction  $f_{em}$  on the other hand, this advantage of the dual-readout method *might also be achieved with only one readout medium*, provided that the time structure of the signals is measured in such a way that the contribution of neutrons can be measured event by event.

In order to check the validity of the above statement, we performed an analysis very similar to the one that was originally

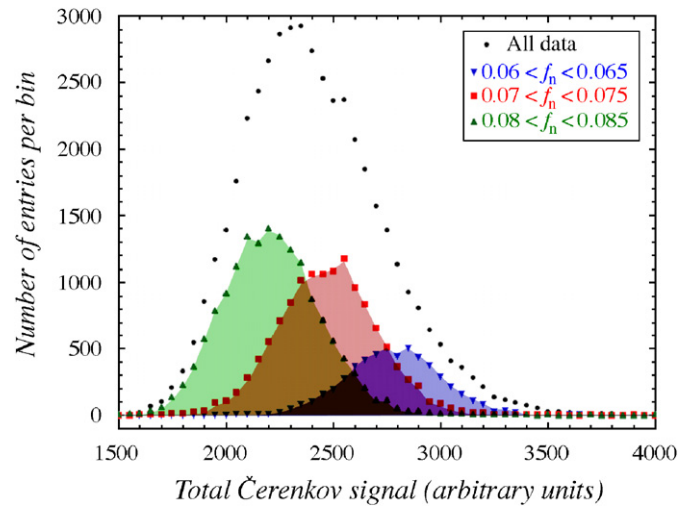


**Fig. 8.** Distribution of the total Cherenkov signal for 200 GeV “jets” and the distributions for three subsets of events selected on the basis of the fractional contribution of neutrons to the scintillator signal.

used to study the merits of the dual-readout method. We selected event samples based on their  $f_n$  value and compared the total signal distributions for these different subsamples and for the entire event sample. Fig. 8 shows an example of the results. The figure contains the total Cherenkov signal distributions for all 200 GeV “jet” events, as well as the distributions for subsamples of events with  $0.06 < f_n < 0.065$  (the blue downward pointing triangles),  $0.07 < f_n < 0.075$  (red squares) and  $0.08 < f_n < 0.085$  (green upward pointing triangles). Clearly, the different subsamples each probe a different region of the total signal distribution for all events. This total Cherenkov signal distribution for all events is thus a superposition of many distributions such as the ones shown in this figure. Each of these distributions for the subsamples has a different mean value, and a resolution that is *substantially better* than that of the overall signal distribution. The signal distributions for the subsamples are also much more Gaussian than the overall signal distribution, whose shape is simply determined by the extent to which different  $f_n$  values occurred in practice. And since the  $f_n$  distribution is skewed to the low side (Fig. 5b), the overall Cherenkov signal distribution is skewed to the high side.

These results are qualitatively very similar to the ones obtained by selecting subsamples of events based on their  $f_{em}$  value, derived from the  $Q/S$  signal ratio [9]. In the next subsection, we investigate to what extent the hadronic calorimetric resolution can be improved by using the measured values of  $f_n$ .

### 3.4. Improving the calorimeter performance through neutron measurements

In order to investigate the relationship between  $f_n$  and the total Cherenkov signal, or between  $f_n$  and the  $Q/S$  signal ratio, we repeated the analysis that led to Fig. 8 systematically for a large number of bins in the  $f_n$  distribution. For each  $f_n$  bin, the mean value of the distribution of these quantities, plus its associated uncertainty were determined. The results for the 200 GeV “jet” event sample are shown in Fig. 9.

They can be described with arithmetic expressions. We found that the relationship between  $f_n$  and  $Q/S$  was reasonably well described by a simple linear function:

$$f_n = 0.110 - 0.077 \frac{Q}{S} \quad (3)$$

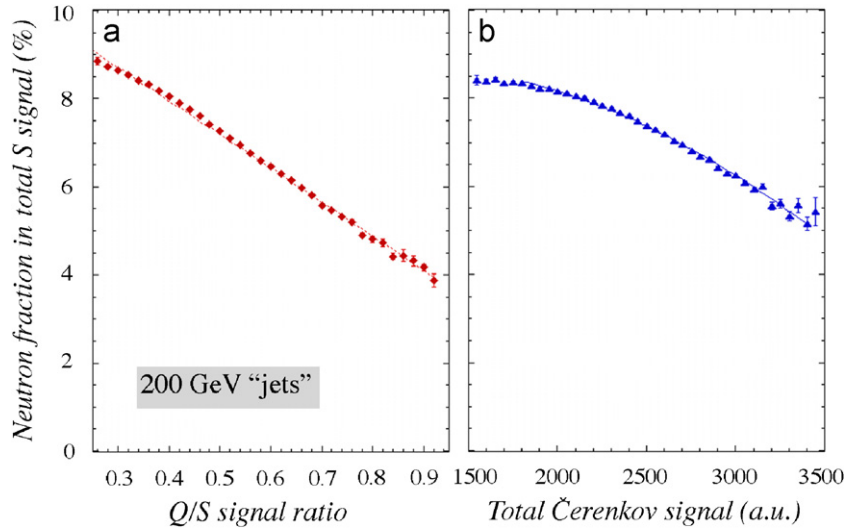


**Fig. 9.** The  $Q/S$  signal ratio (a) and the total Čerenkov signal (b) as a function of the fractional neutron contribution to the total scintillator signal. The neutron fraction was determined according to Eq. (1). Data for 200 GeV “jets”.

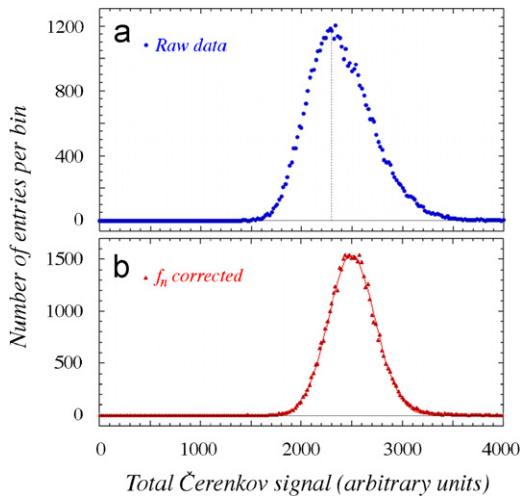


**Fig. 10.** Distribution of the total Čerenkov signal for 200 GeV “jets” before (a) and after (b) applying the correction based on the measured value of  $f_n$ , described in the text.

while the relationship between  $f_n$  and the average Čerenkov signal was well described by a second-order polynomial, in the region  $1800 < Q < 3500$ , which covered  $\approx 99\%$  of the signal (see Fig. 8):

$$f_n = 0.0827 + 0.0119Q - 0.0062Q^2 \quad (4)$$

where  $Q = Q/1000$ . These fits, which are indicated in Fig. 9, made it possible to reconstruct the  $Q/S$  signal ratio (and thus the em shower fraction) and the total Čerenkov signal on the basis of the measured value of  $f_n$ , i.e., on the basis of the measured time structure of the scintillator signals alone.

Fig. 10 illustrates how the energy resolution of the Čerenkov signals could be improved by making use of the measured neutron contribution to the scintillator signals. The figure shows the signal distribution for 200 GeV “jet” events before and after a simple correction based on the measured value of  $f_n$  was made. The measured relationship between the average values of  $f_n$  and the Čerenkov signal (Eq. (4)) was used to correct the measured Čerenkov signal such that the  $f_n$  values of all events were the same (a value of 0.07 was arbitrarily chosen for this purpose).

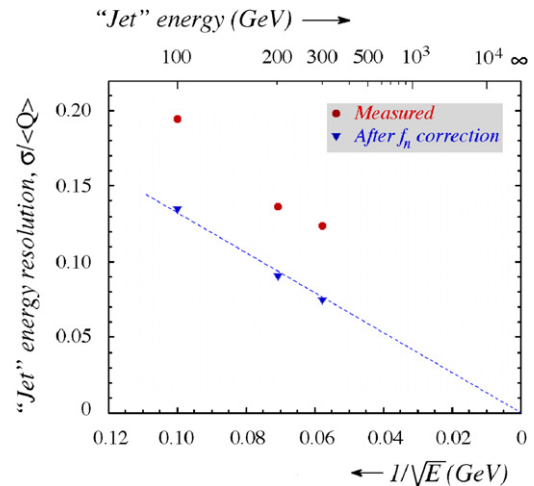


**Fig. 11.** Relative width of the Čerenkov signal distribution for “jets” as a function of energy, before and after a correction that was applied on the basis of the relative contribution of neutrons to the scintillator signals.

Since the Čerenkov signal distribution is the projection of the data points in the scatter plot of Fig. 6 onto the vertical axis, this correction represents the effect of a rotation in the  $f_n/Q$  plane.

The resulting signal distribution is narrower and more symmetric than the measured distribution. It is also well described by a Gaussian function. The energy resolution ( $\sigma_{\text{rms}}$ ) improved from 13.5% to 9.0%.

The same procedure was repeated for the other energies at which “jet” measurements were performed: 100 and 300 GeV. The energy resolution before and after the event-by-event correction based on the measured value of the relative contribution of neutrons to the scintillator signals is shown as a function of the “jet” energy in Fig. 11. Interestingly, after this correction the energy resolution is observed to scale with  $E^{-1/2}$ , as indicated by the dashed line. The corrections made to the signal distributions based on the measured contribution of neutrons to the hadronic scintillator signals thus have eliminated the deviations from  $E^{-1/2}$  scaling typical for non-compensating calorimeters. Whereas these improvements in hadronic energy resolution are certainly remarkable, they are not as impressive as those obtained with a direct measurement of the em shower fraction, through the  $Q/S$

signal ratio in a dual-readout calorimeter [9]. The main reason for this difference is the fact that the resolution is dominated by fluctuations in  $f_{em}$ , and while  $f_{em}$  and  $f_n$  are correlated, this (anti-) correlation is not perfect, as illustrated in Fig. 12.

Perhaps even more important than the improvements in the energy resolution and the shape of the response function is the fact that the event-by-event measurement of the em shower fraction makes it possible to reconstruct the correct hadronic shower energy, in an instrument calibrated with electrons, and achieve hadronic signal linearity in the process. Fig. 12 shows how the em shower fraction could be derived from the measured fractional contribution of neutrons to the hadronic scintillator signals. The linear relationship

$$f_{em} = 1.986 - 22.032f_n \quad (5)$$

derived for 200 GeV “jets” and represented by the straight line in the figure, also gave a reasonable description of the experimental data at other energies. Once the em fraction is known, the shower energy  $E$  can be found from  $f_{em}$  and the measured scintillator

signal  $S_{meas}$ :

$$E = S_{meas} \frac{(e/h)_S}{1 + f_{em}[(e/h)_S - 1]} \quad (6)$$

It can also be found from the measured Cherenkov signal by replacing the  $e/h$  value for the copper/scintillator calorimeter structure  $(e/h)_S$  by that for the copper/quartz structure [9].

Unfortunately, it was not possible to check to what extent this procedure, which was successfully applied before using the directly measured  $f_{em}$  values [9], also worked for  $f_{em}$  values derived from the neutron contribution to the scintillator signals. The main reason for this was the need to be able to correct event-by-event for the (substantial) effects of light attenuation in the fibers on the calorimeter signals. This required that the beam entered the calorimeter at a small, but non-zero angle with the fibers, so that the depth of the light production could be determined from a comparison between the impact point of the particles and the lateral energy deposit pattern [9]. Since the calorimeter was oriented at zero degrees in these tests, this was not possible. However, we do not expect that future tests will show that the applicability of this technique to eliminate non-linearities depends on the way in which  $f_{em}$  is being determined.

### 3.5. Neutrons and the invisible energy

In the previous subsection, we have demonstrated that a measurement of the relative contribution of neutrons to the hadronic scintillator signals offers similar possibilities for correcting the effects of non-compensation as an event-by-event measurement of the em shower fraction. However, when both  $f_{em}$  and  $f_n$  are being measured, even better results may be expected.

The correction described in Eq. (6) accounts *on average* for the invisible energy lost in the shower development process, by equating the hadronic calorimeter signals, on average, to electromagnetic signals of the same energy, i.e., by extrapolating the measured signals to the value expected for  $f_{em} = 1$ . However, if we would select a subsample of hadronic events, all with the same  $f_{em}$  value, there would still be event-by-event differences in the share of invisible energy. The nuclear reactions taking place in the non-em shower development process vary from event to event, and so does the nuclear binding energy lost in these processes. For

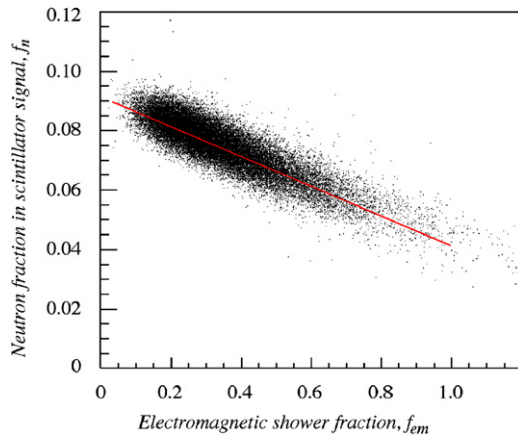


Fig. 12. Relationship between the average fractional contribution of neutrons to the scintillator signals and the em fraction of the showers induced by 200 GeV “jets”.

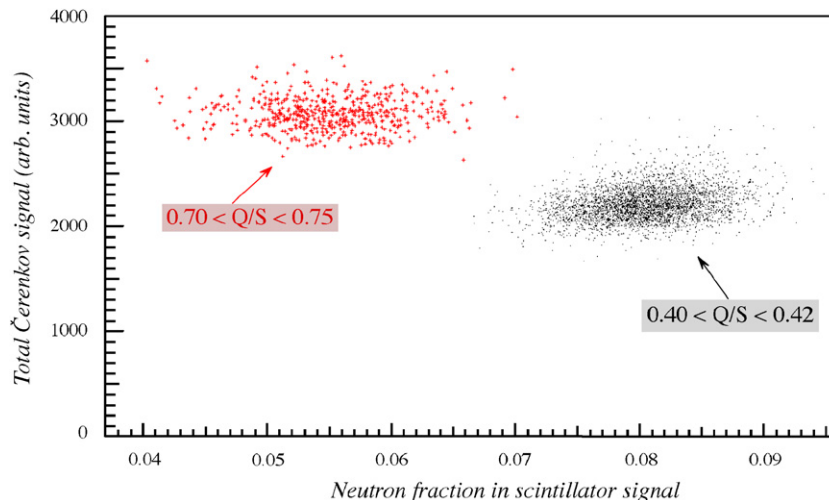
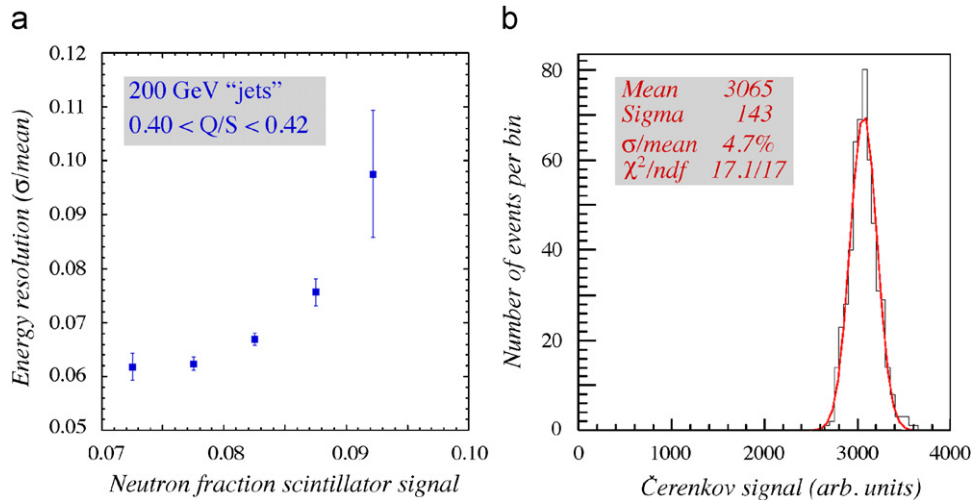


Fig. 13. Scatter plot for 200 GeV “jet” events, all of which have either a  $Q/S$  signal ratio between 0.40 and 0.42 (the black dots), or between 0.70 and 0.75 (the red crosses). For each individual event, the combination of the total Čerenkov signal and the fractional contribution of neutrons to the total scintillator signal is given. The neutron fraction,  $f_n$ , was determined according to Eq. (1).





**Fig. 14.** The energy resolution for 200 GeV “jets” with the same em shower fraction, as a function of the fractional neutron contribution to the scintillator signals (a). Čerenkov signal distribution for 200 GeV “jets” with  $0.70 < Q/S < 0.75$  and  $0.45 < f_n < 0.65$ , together with the results of a Gaussian fit (b).

this reason, in calorimeters such as the DREAM fiber calorimeter, measurements of  $f_n$  provide information *complementary* to that obtained from the  $Q/S$  signal ratio.

This is illustrated in Fig. 13, which shows a scatter plot of  $f_n$  versus the total Čerenkov signal for two subsamples of 200 GeV “jet” events. All event in each subsample have approximately the same  $Q/S$  signal ratio, i.e., the same value of  $f_{em}$ . However, the fractional neutron contribution to the scintillator signals from the events in each subsample differs quite substantially.

Fig. 14a shows that the energy resolution is clearly affected by the relative contribution of these neutrons to the signals. As  $f_n$  increases, so does the fractional width of the Čerenkov signal distribution. A larger  $f_n$  values means that the average invisible energy fraction is larger. This in turn implies that the event-to-event fluctuations in the invisible energy are larger, which translates into a worse energy resolution, even in signals to which the neutrons themselves do not contribute.

Fig. 14b illustrates the quality of the response function that was achieved with the combined information on the em shower fraction and the contribution of neutrons to the signals. This Čerenkov signal distribution concerns 200 GeV “jet” events with a  $Q/S$  value between 0.70 and 0.75 and a fractional neutron contribution to the scintillator signals between 0.045 and 0.065. The distribution is very well described by a Gaussian fit, with an energy resolution of 4.7%. The resolution was further reduced, to 4.4%, when the neutron fraction was narrowed down to 0.05–0.055. As a reminder, we mention that these results were achieved in a calorimeter with an instrumented mass of only about 1 ton. We have measured that the average side leakage for single pions of 200 GeV amounted to  $\sim 10\%$  in the scintillation channel [12]. For our “jets” this fraction is of course even larger. Event-to-event fluctuations in this leakage fraction are most likely an important contribution to the mentioned resolution. The small light yield in the Čerenkov channel (eight photoelectrons per GeV deposited energy [8]) is responsible for another significant contribution: 2.5% at 200 GeV.

Light yield fluctuations could be reduced by using fibers with a larger numerical aperture, a larger packing fraction, light detectors with a larger quantum efficiency, or a combination of these modifications. If they were sufficiently reduced in this way, we believe that in a larger detector of this type, where fluctuations in (side) leakage would be much smaller, event-by-event measurements of  $f_{em}$  and  $f_n$  as described in this paper could

probably further reduce the measured energy resolution to values close to the theoretical limit mentioned in Section 1.

#### 4. Conclusions

The performance of almost all hadron calorimeters used in practice is determined, limited and spoiled by fluctuations in the em shower fraction,  $f_{em}$ . Dual-readout calorimeters in which the scintillation and Čerenkov light generated in such showers are measured simultaneously, make it possible to measure the value of  $f_{em}$  for each event, and thus eliminate the effects of these fluctuations. In this paper, we have demonstrated that it is to some extent possible to achieve similar results with only one type of readout (plastic scintillating fibers), by measuring the time structure of the signals. The relative contribution of soft neutrons to these signals is anti-correlated to  $f_{em}$ . This contribution is derived from the characteristic exponential tail in the time structure of the signals. However, the results obtained with this method are not as good as those from a dual-readout calorimeter, in which the value of  $f_{em}$  is explicitly measured.

We have also demonstrated that a measurement of the contribution of neutrons to the scintillator signals provides information that is complementary to that obtained from an independent measurement of  $f_{em}$ . This complementary information makes it possible to further improve the hadronic performance of dual-readout calorimeters.

When the experiments described in this paper were being planned, we did not expect to find that measurements of the time structure of the DREAM signals would turn out to be so useful. For that reason, the experimental setup was not as perfect as it could have been. Among the issues that could be improved, we mention:

- Elimination of the Linear Adders. Measurement of the time structure of all individual signals would avoid potential problems (such as reflections created by small impedance mismatches), and would also offer the possibility to measure the energy deposit profile. Moreover, the time structure of the *entire* calorimeter signal would be measured, including the three towers whose Čerenkov signals were left out in the present measurements.
- Orientation of the calorimeter at a small angle with the beam. This would make it possible to eliminate the effects of light attenuation

in the fibers on the calorimeter signals and thus check the linearity that could be achieved with measurements of  $f_n$  alone.

We are planning follow-up measurements in which these improvements will be implemented.

### Acknowledgments

We thank CERN for making particle beams of excellent quality available. This study was carried out with financial support of the United States Department of Energy, under contract DE-FG02-07ER41495.

### References

- [1] R. Wigmans, *Calorimetry—Energy Measurement in Particle Physics*, International Series of Monographs on Physics, vol. 107, Oxford University Press, Oxford, 2000.
- [2] U. Behrens, et al., *Nucl. Instr. and Meth. A* 289 (1990) 115.
- [3] D. Acosta, et al., *Nucl. Instr. and Meth. A* 308 (1991) 481.
- [4] J. Brau, T.A. Gabriel, *Nucl. Instr. and Meth. A* 238 (1985) 489.
- [5] S. Aronson, et al., *Nucl. Instr. and Meth. A* 269 (1988) 492.
- [6] G. Drews, et al., *Nucl. Instr. and Meth. A* 290 (1990) 335.
- [7] N. Akchurin, et al., *Nucl. Instr. and Meth. A* 581 (2007) 643.
- [8] N. Akchurin, et al., *Nucl. Instr. and Meth. A* 536 (2005) 29.
- [9] N. Akchurin, et al., *Nucl. Instr. and Meth. A* 537 (2005) 537.
- [10] N. Akchurin, et al., *Nucl. Instr. and Meth. A* 533 (2004) 305.
- [11] D.R. Winn, W.A. Worstell, *IEEE Trans. Nucl. Sci.* NS-36 (1) (1989) 334.
- [12] N. Akchurin, et al., *Nucl. Instr. and Meth. A* 584 (2008) 273.